2018

# Surfactant Driven Assembly of Freeze-casted, Polymer-derived Ceramic Nanoparticles on Grapehene Oxide Sheets for Lithium-ion Battery Anodes

Ali Zein Khater
*University of Central Florida*

# SURFACTANT DRIVEN ASSEMBLY OF FREEZE-CASTED, POLYMER-DERIVED CERAMIC NANOPARTICLES ON GRAPHENE OXIDE SHEETS FOR LITHIUM ION BATTERY ANODES

by

Ali Zein Khater

A thesis submitted in partial fulfillment of the requirements
for the Honors in the Major Program in Physics
in the College of Sciences
and in the Burnett Honors College
at the University of Central Florida
Orlando, Florida

Spring Term, 2018

Thesis Chairs: Laurene Tetard, Ph.D. and Lei Zhai, Ph.D.

# ABSTRACT

Traditional Lithium-Ion Batteries (LIBs) are a reliable and cost-efficient choice for energy storage. LIBs offer high energy density and low self-discharge. Recent developments in electric-based technologies push for replacing historically used Lead-Acid batteries with LIBs. However, LIBs do not yet meet the demands of modern technology. Silicon and graphene oxide (GO) have been identified as promising replacements to improve anode materials. Graphene oxide has a unique sheet-like structure that provides a mechanically stable, light weight material for LIB anodes. Due to its structure, reduced graphene oxide (rGO) is efficiently conductive and resistive to environmental changes. On the other hand, silicon-based anode materials offer the highest theoretical energy density and a high Li-ion loading capacity of various elements [20]. Silicon-based anodes that have previously been studied demonstrated extreme volumetric expansion over long cycles due to lithiation. Polysiloxane may be an interesting alternative as it is a Si-based material that can retain the high Li-ion loading capacity of Si while lacking the unattractive volumetric expansions of Si. Polymer derived ceramic-decorated graphene oxide anodes have been suggested to increase loading capacity, thermal resistance, power density, and mechanical stability of LIBs. Coupled with mechanically stable graphene oxide, polymer derived ceramic nanoparticle decorated graphene oxide anodes are studied to establish their efficiencies under operating conditions.

# DEDICATION

Firstly, I dedicate my work to Allah, the Exalted, Lord of the worlds.

Also, to the ladies of my life and, especially, my wife, my greatest support and the reason behind my smile.
And last but never least; my family for their endless prayers and encouragement.

# ACKNOWLEDGEMENTS

Firstly, I would like to thank Dr. Lei Zhai for giving me the excellent opportunity to succeed, excel, and lead with his guidance and support.
I would like to thank Dr. Laurene Tetard for her guidance and encouragement.
It was an honor to have them both as advisors.
Thank you for your assistance and support. The experience you have passed on to me is incomparable, surely it will lead to my success in my future journeys.

To my wife, I love you and thank you for sacrificing our time together so that I may excel. Thank you for supporting me and thank you for being my best friend.

I would also like to thank my entire family for their endless support and prayers. Thank you for being my strength. To my parents who gave me the world, thank you for guidance to success.

I would like to recognize everyone in the laboratory who supported me in my endeavors, provided me with new expertise, and great friendships and great memories.

I would like to give special recognition to David Fox for his support and mentorship throughout the project and a great friendship.

I would like to recognize those who partially supported this work.

Partial support for this work was provided by the National Science Foundation Scholarships in Science, Technology, Engineering, and Mathematics (S--STEM) program under Award No. 1356233. Any opinions, findings, and conclusions and recommendations expressed in this material are those of the author(s) and do not necessarily reflect the views of the National Science Foundation
DUKE Energy and BOEING provided partial funding for this work
And partial funding from the NSF-Funded EXCEL/COMPASS Program

# TABLE OF CONTENTS

**INTRODUCTION** ..... **1**

**METHODS** ..... **7**

Graphene Oxide Synthesis ..... 7

Graphene Oxide Aerogel Fabrication ..... 9

Polymer Derived Ceramic Nanoparticles on Graphene Oxide Sheets ..... 10

Aerogel Pyrolysis ..... 11

Anode Fabrication, Battery and Capacitor Assembly. ..... 12

**DISCUSSION** ..... **14**

**CONCLUSION** ..... **21**

**REFERENCES** ..... **23**

# TABLE OF FIGURES

FIGURE 1: GRAPHENE OXIDE FORMATION ..... 7

FIGURE 2: ASSEMBLY OF A COIN CELL FOR LIB ANODE TESTING ..... 12

FIGURE 3: CHARACTERIATION OF THE SYNTHESIZED MATERIALS USING SCANNING ELECTRON MICROSCOPY. ..... 15

FIGURE 4: CHARACTERIATION OF THE SYNTHESIZED MATERIALS USING HIGH RESOLUTION TRANSMISSION ELECTRON MICROSCOPY ..... 15

FIGURE 5: CHARACTERIZATION OF THE COMPOSITION OF THE NANOPARTICLES WITH ELEMENTAL ANALYSIS ..... 16

FIGURE 6: CHARACTERIZATION OF THE THICKNESS OF GO FLAKES SYNTHESIZED ..... 17

FIGURE 7: PERFORMANCE OF THE NEW NANOPARTICLE LOADED RGO ANODE IN CYCLIC VOLTAMETRY TESTING ..... **ERROR! BOOKMARK NOT DEFINED.**

FIGURE 8. PERFORMANCE OF THE NEW NANOPARTICLE LOADED PARALLEL PLATE CAPACITOR TESTING ..... 20

# INTRODUCTION

The demand for high power, high loading capacity rechargeable batteries is on the rise due to advancements in industrial electronics such as electric vehicles, renewable energy technology, and at-home electronics. Over the last 25 years (since the commercialization of the first Lithium-ion batteries), research publications and patents regarding Lithium-ion batteries (LIBs) have increased almost exponentially [20]. Due to the large flux of research dedicated to reaching a deeper understanding LIBs, there is a good understanding about the mechanisms driving their performance [1,2,12,13,17,22,23,25,31,35]. Lithium-ion batteries constitute a promising solution to meet the growing demand for industrial energy storage problems due to their unique properties [6,8,11,20,25,27,29]. Furthermore, the advancements in nanoscience and technology and the understanding of the behavior of various materials have made it possible to bring out advances in battery technology. In particular, efforts are concentrated on developing high energy density and long cycle devices [1,7,18,30,31,32,33]. Various configurations of LIBs have been devised to adapt to different technologies including environmentally-friendly devices, flexible electronics, automobiles, and other technologies [1,7,6]. Typical areas of optimization pertain to the modification of the anode, cathode, or electrolyte composites [1,6,7,9,11,17,18,29-33], or to adjusting other components in the LIBs [1,6,7,9,11,17,18,29-33].

Anode composition optimization is a hopeful solution to improve LIB performance, specifically, to increase the lithium-ion loading capacity of the anode material. Lithium-ion battery anodes typically operate on lithium-ion alloying reactions in which Li-ions intercalate into the

carbon matrix of the anode device. Standard LIB anode devices are comprised of carbon-based materials such as graphite or graphite oxide [6,20,34]. Carbon materials such as graphite are utilized for anode material due to their properties as a highly conductive material, high loading capacity and gravimetric capacity, and eco-friendly nature.

Graphitic anodes have a high specific capacity (~360 mAh $g^{-1}$). Although this has been sufficient for previous technologies, modern applications are rapidly making these battery devices obsolete. Furthermore, graphite is difficult to process without hazardous solvents, as it does not disperse in water. Graphene oxide (GO), on the other hand, retains similar properties of graphite but is easily processed in water, making it a highly appealing graphite material replacement for industrial application. Thermal reduction of GO (rGO) produces a highly conductive material. Coupled with a clean processing method and impressive electrical, thermal, and mechanical properties under high stress conditions, rGO is a strong candidate for the replacement for graphite in anode technology.

To keep up with clean energy technology and high power usage at-home devices, high energy density energy-storage devices are needed. Adaptations to the generic graphite anode and alternative anode materials have been proposed and studied to increase the loading capacity of anode devices [1,32]. In developing anode devices, a range of obstacles are presented before LIB efficiency can be optimized [12,35]. Silicon is an attractive candidate for anode optimization as it offers impressive properties [17,20] including high Lithium-ion loading and gravimetric capacities, natural abundance, and cost efficient. Amongst a range of elements, Si has the highest theoretical energy density, gravimetric capacity and loading capacity. In addition, Si is abundant in nature, environmentally benign, and cost efficient. Unfortunately, over long cycle lithiation

charge and discharge, Si anodes are subjected to large volumetric expansion above 400% [4]. While Si delivers a theoretical loading capacity of 4200 mAh $g^{-1}$ [25,27,30], volumetric expansion of Si anodes renders devices industrially inviable devices due to gradual fragmentation of the active material layers [17,21,32]. Continuous fracturing over long cycles caused by stress during application results in continuously forming new solid electrolyte interface (SEI) [8,25,27,28,32]. Thus, alternative solutions are still in need. Solutions to resolve the issue of volumetric expansion of Si anodes have been proposed such as adjusting Si particle size and shape [13,16,21].

Due to Si's impressive characteristics, researchers are actively engaged in overcoming the problem of volumetric expansion, and many solutions have been proposed [7,16]. While Si-based anodes have shown promise, it is clear that there is small potential for industrial application to date, and alternative solutions should be considered. Amorphous Si structures hold some promise to replace pure Si based anodes. In this case, the properties of Si such as high loading capacity and thermal and mechanical stability are retained while acquiring another attractive quality not present in pure Si-based anodes i.e. reversible lithiation over long cycles with minimal volumetric expansion [7]. Silicon oxycarbide (SiOC) also exhibits the conditions to satisfy high loading capacity while maintaining minimal volumetric expansion over long cycle lithiation and de-lithiation. SiOC anode devices have previously been devised demonstrating impressive anode performance for long cycle, high loading capacity [7,18,29,33]. While SiOC has the potential to resolve the issues posed before, previously proposed methods require heavy industrial processing techniques such as ball-milling and chemical reaction methods that span over the course of hours with limited control of SiOC particle size and dispersion. Such processes may not be appealing for industrial application due to lack of SiOC size and dispersion control, expensive equipment

required, or long fabrication times. It is evident, however, that SiOC are hopeful substitutes for Si-based anodes.

Similar to carbon matrices, SiOC anodes operate on a similar process of alloying reaction anodes. Although the process is not quite the same as in a carbon matrix, the general lithiation process occurs similarly. The properties of carbon materials are unique and complement Si. The mechanical integrity, thermal stability, and electrical properties of rGO provide an interesting complementing material for SiOC. rGO exhibits impressive electrical conductivity similar to that of graphite while being dispersible in water. These properties can be used to complement the high loading capacity of SiOC. SiOC utilized in a carbon matrix can be used to enhance anode devices. Contrary to standard Si-Carbon anodes, Carbon-SiOC anodes will not experience volumetric expansion that will compromise the integrity of the electrode device due to the glassy structure of SiOC. This unique combination of materials could potentially deliver a high loading capacity device with high electrical conductivity.

Polysiloxane oligomers can be pyrolyzed to form amorphous glassy structures. As formerly mentioned, these amorphous glassy structures are mechanically stable and will not experience the same extreme volumetric changes as Si over long cycle lithiation. It is possible to avoid formerly mentioned methods such as ball milling or chemical processes through the emulsification of polysiloxane. Sodium dodecyl sulfate (SDS) is a surfactant capable of creating microemulsions. For the purpose of this study, SDS is used as a compatibilizing agent to disperse microemulsions of polysiloxane in water. Thermal reduction through pyrolysis disposes of organic molecules in polysiloxane and SDS resulting in a ceramic SiOC-S-Na glassy compound with high Li-loading capacity. Microemulsion technology alone cannot successfully deliver the desired product of SiOC

nanoparticles on GO. A combination of surfactant science and freeze casting is critical in molding SiOC-S-Na structures on GO.

Freeze casting is a simple technique to produce porous complex-shaped ceramic or polymeric parts [9,10]. Freeze casting utilizes a ceramic slurry poured into a mold and frozen. Graphene oxide sheets act as a scaffold. The solvent binds to the scaffold. The polymer slurry is subjected to sublimation during freeze drying under vacuum. Freeze drying avoids the normal stresses and shrinkage that may occur under normal drying conditions. Such stresses can lead to warped or cracked structures. Thermal treatment of the resulting dried sample hardens the material and the heat treated material exhibits improved strength, stiffness, and porosity [9]. Controlling the direction of growth of the ice crystals is critical in controlling the orientation of the porosity [14]. This paper utilizes a common vertical freeze drying technique highlighted through aerogel fabrication [34]. Aerogels are utilized to control the growth of ice crystals. Vertical freeze drying of aerogels is also used to exfoliate graphene oxide sheets. Separation of sheets during freeze drying is critical to allow full exposure of each GO sheet to any treatment of interest: in this case, SiOC nanoparticles. It is important to observe the role played by the freeze drying process and the importance of micellar structures. Unlike a polymeric slurry that will bind to the walls of GO, a micellar solution will isolate individual sections of polysiloxane. The sections are pressed and glued to the walls of GO by the force of the ice crystals in isolated regions across the carbon matrix. The unique combination of techniques results in a quick process to produce nanostructures on the surface of graphene sheets. As the aerogel freeze dries under vacuum, the sections of polymeric material are pulled off the surface of the GO sheets. Under thermal treatment, polysiloxane micelles crosslink into a solid, glassy structure. The amorphous siloxane finds the lowest energy

state and forms spheroidal structures bound chemically to the surface of the graphene oxide matrix. With increasing temperature, polysiloxane is cross linked at 160 $^{o}$C [19,26]. Continuous temperature treatment of the solid material results in a ceramic SiOC-S-Na structure upon pyrolysis. Similarly graphene oxide is reduced at 1000 $^{o}$C leaving a conductive scaffold for with high Li-ion loading capacity. Thus we present a novel and simple method that combines two well-known chemical techniques to avoid ball-milling and time-consuming chemical techniques.

# METHODS

## Graphene Oxide Synthesis

**Material.** Graphite powder, sulfuric acid, potassium permanganate, crushed ice, nanopure water.

**Equipment.** 250 mL round bottom flask, 3-neck flask, oil bath, two magnetic stir bars, thermometer, separatory funnel.

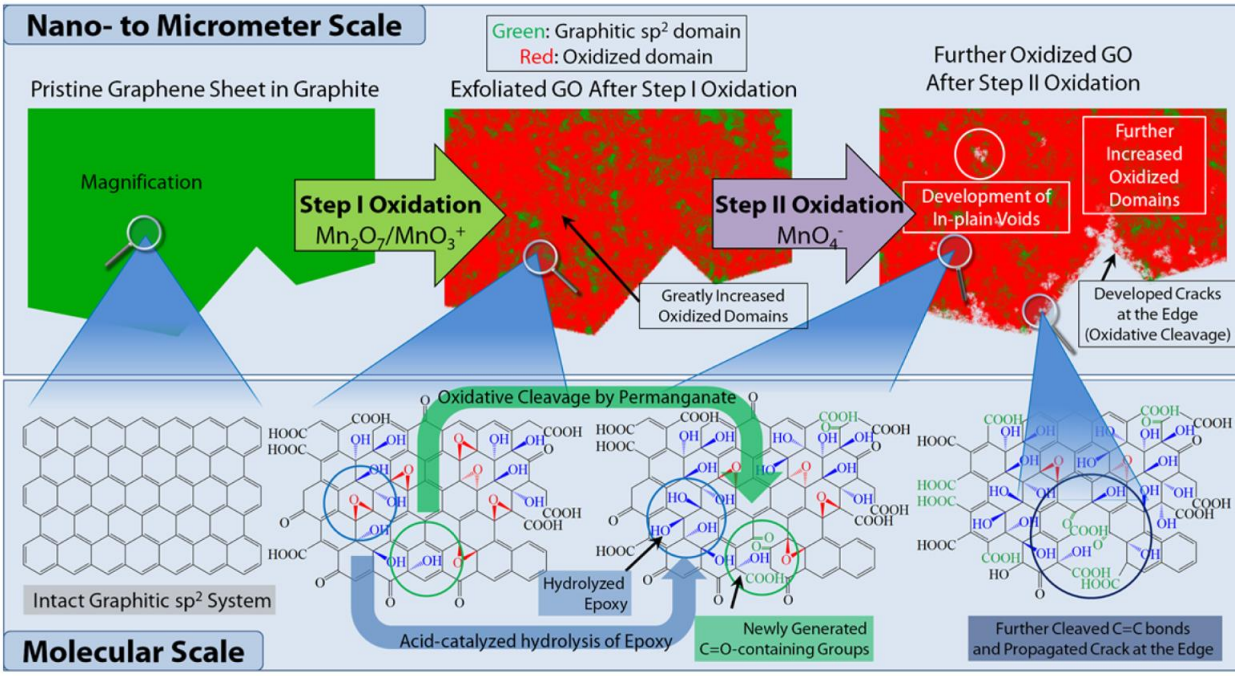


*Figure 1: Graphene Oxide Oxidation Steps highlighting the differences between the water free and water addition oxidation steps. [15]*

**Synthesis.** This method employed a two-step oxidation process in which potassium permanganate was utilized to oxidize large sheets of graphite turning it in graphite oxide. The primary oxidation procedure is understood as the oxidative exfoliation of graphite by dimanganese heptoxide which is the reaction product of potassium permanganate with sulfuric acid resulting in the first step oxidation [15]. Permangynol cations are formed upon addition of water resulting in the second

stage oxidation of graphite oxide [15], as outlined in Figure 1. This step should be limited in time due to its lowering of the conductivity of rGO [15].

Next, a modified Hummer's method was employed. While in an ice bath sitting over a magnetic stir bar, graphite powder was dissolved in sulfuric acid for 5 minutes to allow the intercalation of sulfuric acid between graphite flakes in a 250 mL 3-neck flask, with a magnetic stir bar in the solution to promote the graphite powder to fully disperse in solution (note: a thermometer was placed inside one of the necks to observe temperature fluctuations). Over a period of 10 minutes, potassium permanganate ($KMnO_4$) was slowly added while the stir bar was at a medium spin rate.

After the $KMnO_4$ was added, the beaker was removed from the ice bath and placed over a preheated oil bath; the oil bath was heated to a temperature of ~65 $^oC$. This elevated the temperature of the solution slightly above room temperature, and the selected temperature will be used for the following step. The flask is monitored at ~ 30 $^oC$ for one hour.

80 grams of ice were slowly added over 10 minutes maintaining the temperature of the vessel at ~40$^oC$. 6 mL of hydrogen peroxide was added slowly to the reaction. A violent fizzing occurred and the color of the solution turned to green. The solution was stirred at room temperature for 5 minutes before being purified using centrifugation over several rinses until the pH is over 5. The GO pellets were redisposed in water, frozen, and freeze dried by lyophilizing.

Dried GO was dispersed in nanopure water. The concentration in this step varied between ~200 mg of GO in 250 mL of nanopure water to ~750 mg of GO in 250 mL of nanopure water, typically. The concentration is not important in the GO separation, however, an over concentrated solution is not desirable as it may lead to difficulty in separating the different sized sheets of GO.

The solution was sonicated using a horn sonicator for 10 minutes while pipetting the solution onto the horn sonicator probe to ensure full dispersion of the GO. The solution was covered with parafilm and allowed to settle for 24 hours. Using an ordinary pipette, the top layers were carefully separated from the settled material. The top layers were notably less viscous than the settled material. Optical microscopy presented in Figure 6(A and B) of the separated solution illustrates the GO quality. Evidently, multilayer, aggregated GO sheets and crumpled GO, crashed to the bottom due to their larger mass, while, large single and few layered GO sheets stayed in the top layers of the solution. Thin films of both the many-layer GO (MLGO, Figure 6A) and the -single layer GO (SLGO, Figure 6B) on glass slides produced by drop casting were imaged using optical microscopy.

A 0.5 mg/mL solution of MLGO and SLGO were prepared by sonication for 5 minutes. One drop of solution was drop casted on a glass slide. While the MLGO produced poor quality films, the SLGO rendered a stunningly continuous.

## Graphene Oxide Aerogel Fabrication

**Material.** Graphene Oxide, nanopure water, dry ice.

**Equipment.** Horn sonicator, 20 mL scintillator vial, 2 mL vial, 1 mL micropipette, flat steel plate, aluminum foil.

**Fabrication.** A 20 mg/mL solution of GO was prepared. The solution was mechanically stirred. Using horn sonication, the solution was sonicated for 10 minutes at 10% amplitude. A pipette was used to stir the solution while sonicating.

Half of the GO solution was placed in a new scintillator vial with a magnetic stir bar and was diluted to 10 mg/mL for aerogel fabrication. The solution was stirred using the magnetic stir bar for 10 minutes. 1 mL of 10 mg/mL SLGO was pipetted slowly using a 1 mL micropipette. Due to the natural surfactant properties of GO, a rushed pipetting technique may produce excessive bubbles in the solution rendering parts of the solution useless. When placing the 1 mL of 10 mg/mL GO in the scintillator vial, it was important to quickly eliminate any bubbles that form in the 2 mL vial. To maintain a well dispersed solution and produce equally dense aerogels, the solution should be pipetted immediately after being stirred. After being placed in the 2 mL vial, the vials should be placed on dry ice. A flat surface between the vials and the dry ice can be established by using a thin steel plate wrapped in aluminum. This allowed the aerogels to freeze with vertically grown, exfoliated GO sheets [34].

### Polymer Derived Ceramic Nanoparticles on Graphene Oxide Sheets

**Material.** Polysiloxane, sodium dodecyl sulfate (SDS), nanopure water.

**Equipment.** Horn sonicator, scintillator vial, micropipette, magnetic stir bar.

**Production.** 200 mg of polysiloxane was weighted in a scintillator vial. Polysiloxane was made miscible in water by adding SDS over the measured polysiloxane, typically, 200 mg of polysiloxane for 1 g of SDS. This ratio can be modified to vary the shape and size of the particles, however, because this system also operates according to the properties of freeze casting, the surfactant concentration does not follow typical surfactant recipes [30] and the control of the shape and size of the nanoparticles is difficult. This has not been studied in the scope of this project. 10 mL of nanopure water was added to the solution and then sonicated for 45 minutes and 10%

amplitude. The solution was given time to reach an equilibrium point over 24 hours and was then re-sonicated for 45 minutes. The solution obtained was homogenous. If the solution is not used at the time of sonication, then, additional sonication of 5 minutes should be performed before use. Note that the solution will feel warm to the touch after sonication, which is desired as it allows the polysiloxane to decrease in viscosity.

Using a secondary scintillator vial, 0.5 mL of the prepared polysiloxane solution and 0.5 mL of the prepared GO solution were combined. GO was gently added so as to avoid foaming. Interchangeably 1:1 GO:polysiloxane solutions were added until the desired volume of solution was reached. Using a magnetic stir bar, the solution was stirred for 10 minutes to allow an even dispersion of GO and polysiloxane micelles. Polysiloxane coated GO aerogels followed the same procedure as previously described.

## Aerogel Pyrolysis

**Material.** Freeze dried aerogels.

**Equipment.** Tube Furnace, argon gas, quartz boat.

**Procedure.** The mass of each aerogel was recorded before pyrolysis. The average mass before and after pyrolysis was compared. The aerogels were placed in a quartz boat for treatment in the tube furnace. The tube was filled with argon gas. The temperature in the tube was increased at a rate of 2 $^{o}$C per minute until the temperature in the tube reaches 400 $^{o}$C. It was then kept constant at 400$^{o}$C for one hour. It is important to increment in the first stages of thermal treatment to allow the aerogels and their respective components to off gas. We note that SiOC cross-linked around 160 $^{o}$C and formed a ceramic structure between 350 – 400 $^{o}$C [19,26]. This is more critical for the

nanoparticle loaded aerogels than the GO aerogels, however, for consistency, the same process was repeated for both the GO and nanoparticle load GO aerogels. After one hour, the temperature was increased to 1000 $^{o}$C at 20 $^{o}$C per minute. The temperature was held at 1000$^{o}$C for one hour to assure the complete pyrolysis of GO and polysiloxane.

### Anode Fabrication, Battery and Capacitor Assembly.

**Material.** Graphene oxide aerogels, polysiloxane, graphene oxide coated aerogels, carbon black, polyvinylidine fluoride (PVDF), N-Methyl-2-Pyrrolidone, aluminum foil, copper foil, Lithium metal plate, steel spring, $LiPF_6$, KOH, separator, steel coin cell caps.

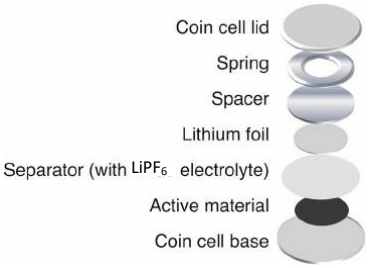


*Figure 2: Coin cell assembly diagram. The active material is the anode composite. The image is adapted from Birkl, Christoph [34].*

**Equipment.** Battery cycle tester, coin cell press.

**Procedure.** Polymer-derived ceramic nanoparticle loaded rGO aerogels were weighed and ground with a pestle and mortar with PVDF and carbon black. The anode data presented utilizes a composite of 10 wt% PVDF and 10 wt% carbon black with 80 wt% aerogel material. Carbon black was used as a conductive network, improving the results from previous trials using anodes with tert-butanol dissolved polysiloxane. The results are presented in the Discussion section. The finely ground powder was dispersed in NMP and put over an aluminum current collector. The composite was dried over night at 80 $^{o}$C. In future experiments, the concentration of nanoparticle loaded rGO sheets to uncoated rGO sheets should be considered, together with drying the material over the copper foil.

In a similar method, a capacitor was fabricated using two electrodes of pure nanoparticle loaded rGO. Instead of grinding the aerogel however, it was found that the material readily disperses in NMP.

# DISCUSSION

Scanning electron microscopy (SEM), presented in Figure 3, was performed to observe the successful loading of nanoparticles onto graphene oxide. Based on these images, it is evident that micellar structures or freeze-casting do not alone result in the formation of nanoparticles on the surface of GO, but rather, the combination of freeze casting the polysiloxane micelles onto the carbon matrix followed by the sequential pyrolysis of the material on the surface made the nanoparticle formation possible. This is further supported by the evidence from dissolving polysiloxane in tert-butanol. Polysiloxane dissolved in tert-butanol resulted in a freeze-casted mold. Unlike the micellar solution, however, the polymer slurry did not form nanoparticles on the carbon scaffolds, as seen in Figure 3(G-I). Therefore, the combination of a micro-emulsified polysiloxane and freeze-casting gave way to polymer derived ceramic nanoparticle loading on graphene oxide sheets.

Two characterization techniques were employed to verify the nanoparticle composition – energy dispersive x-ray spectroscopy (EDS) and electron energy loss spectroscopy (EELS). The characterization of particles on the surface reveals the composition of the particles to have high concentrations of carbon, oxygen, and silicon, as shown in Figure 5. Although the nanoparticles are expected to be rich in carbon and oxygen, there is room to increase the ratio of carbon and oxygen to silicon by modifying the surfactant. Silicon-based surfactants may be good candidates

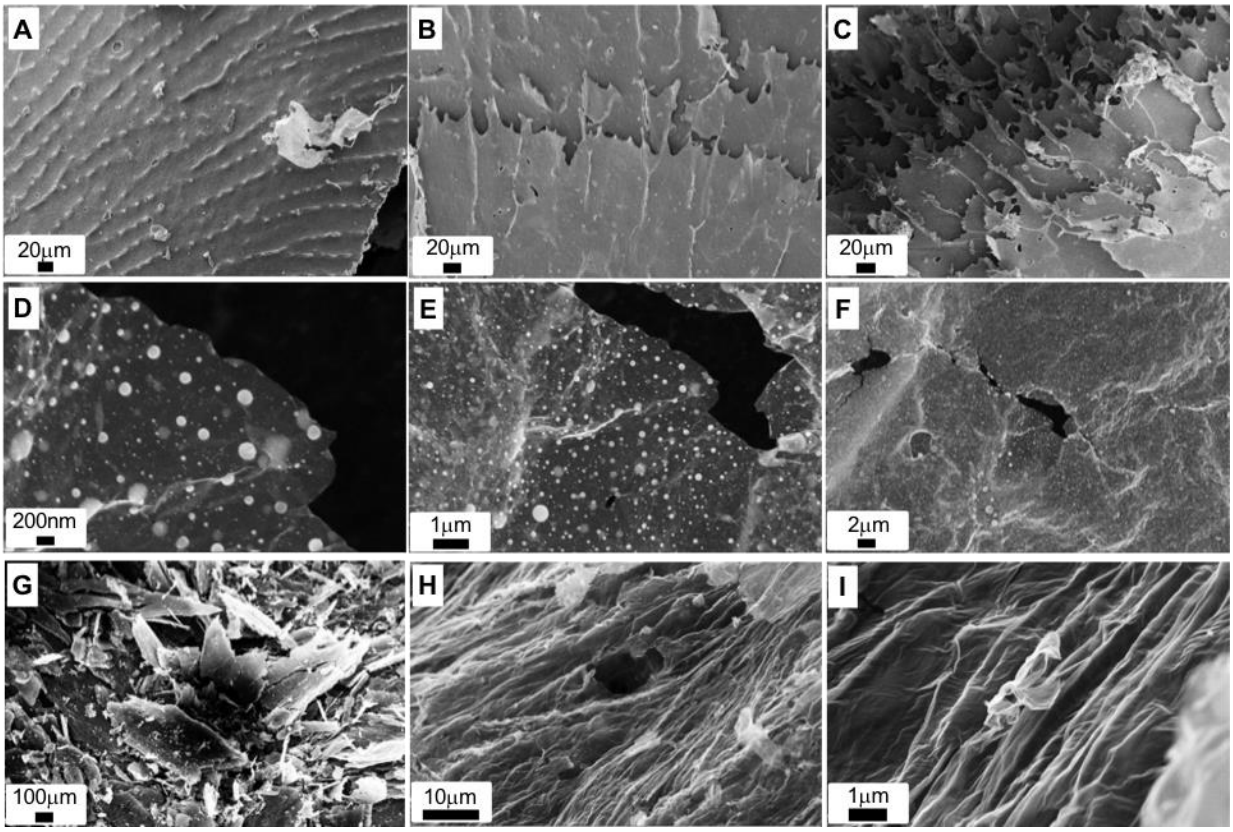


*Figure 3: SEM Images of GO aerogels before reduction (A-C) and after reduction at 1000 oC (D-F). SEM images of materials obtained by dissolving polysiloxane in tert-butanol (G-I).*

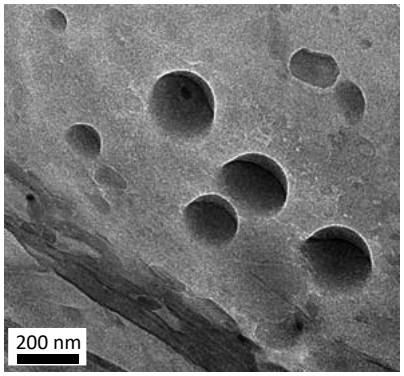


*Figure 4: High resolution TEM was employed to observe the contact between the polymer derived ceramic nanoparticles and the graphene oxide*

for this. Currently, SDS leaves behind trace amounts of sodium and sulfur. Although it may be interesting to incorporate sodium and sulfur into the material in some applications, it is not of interest for the scope of this project. In the future, it may be interesting to explore alternative surfactants to disperse polysiloxane in solution to minimize the quantities of Na and S. Both EDS and EELS show that there is a clear distinction between the carbon matrix

background and the nanoparticles studied. In some regions, large aggregates of nanoparticles agglomerate

Based on our observations, we surmise that a more comprehensive study of the concentration of polysiloxane emulsions to GO should be conducted in future studies to evaluate the optimum conditions for a polydispersed solution. By modifying the concentration of the SDS or other surfactants, it is also hypothesized that the size of the nanoparticles could be modified and controlled. High resolution tunneling electron microscopy images were collected to study the interaction of the nanoparticles and the GO surface (Figure 4). However, further tests are required to determine the nature of the interaction.

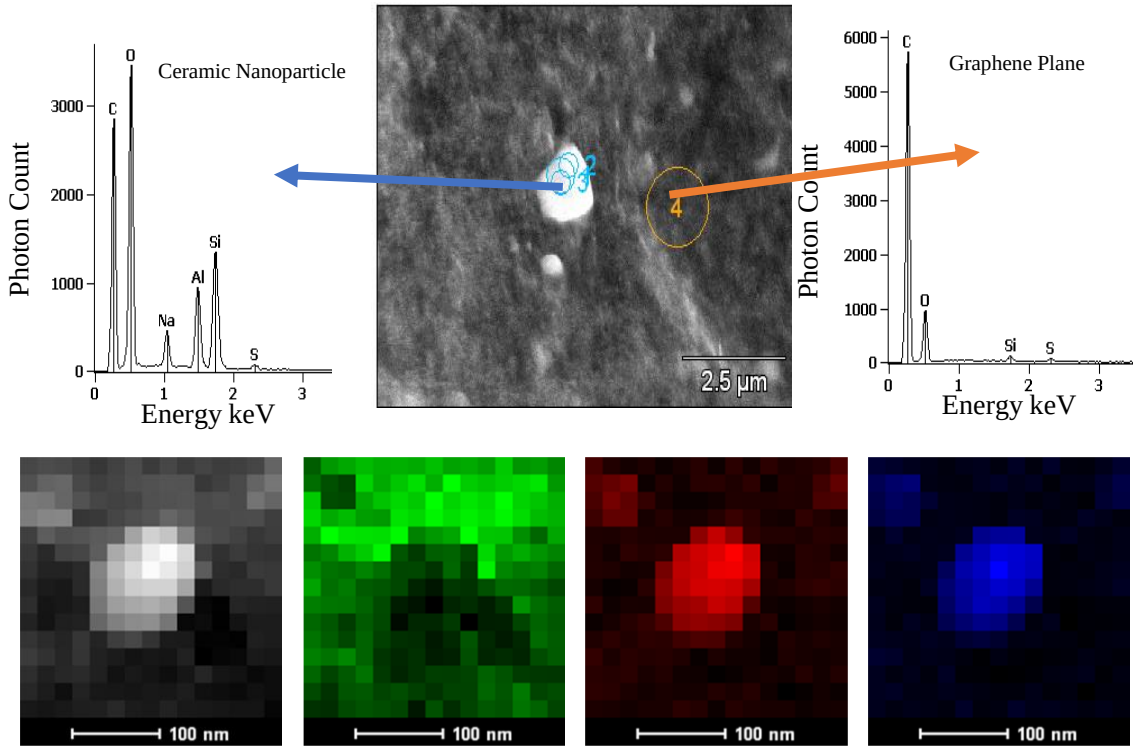


*Figure 5: Energy Dispersive X-Ray Spectroscopy (**top**) give an elemental analysis of the compound and Electron Energy Loss Spectroscopy (**bottom**) confirms the findings of EDS and give an understanding of the dispersion of different elements in the particle: particle image=gray, carbon=green, silicon=red, oxygen=blue.*

A crucial portion of this thesis depended on the graphene oxide synthesized in the laboratory. In an effort to optimize the coating of GO sheets, the synthesis of single-layer GO was attempted. An interesting approach was discovered in studying the synthesized GO. The presented method for GO synthesis yielded a large volume of GO, half of which was MLGO, which appeared crumpled GO sheets under optical microscopy presented in Figure 6A. After the GO synthesis was

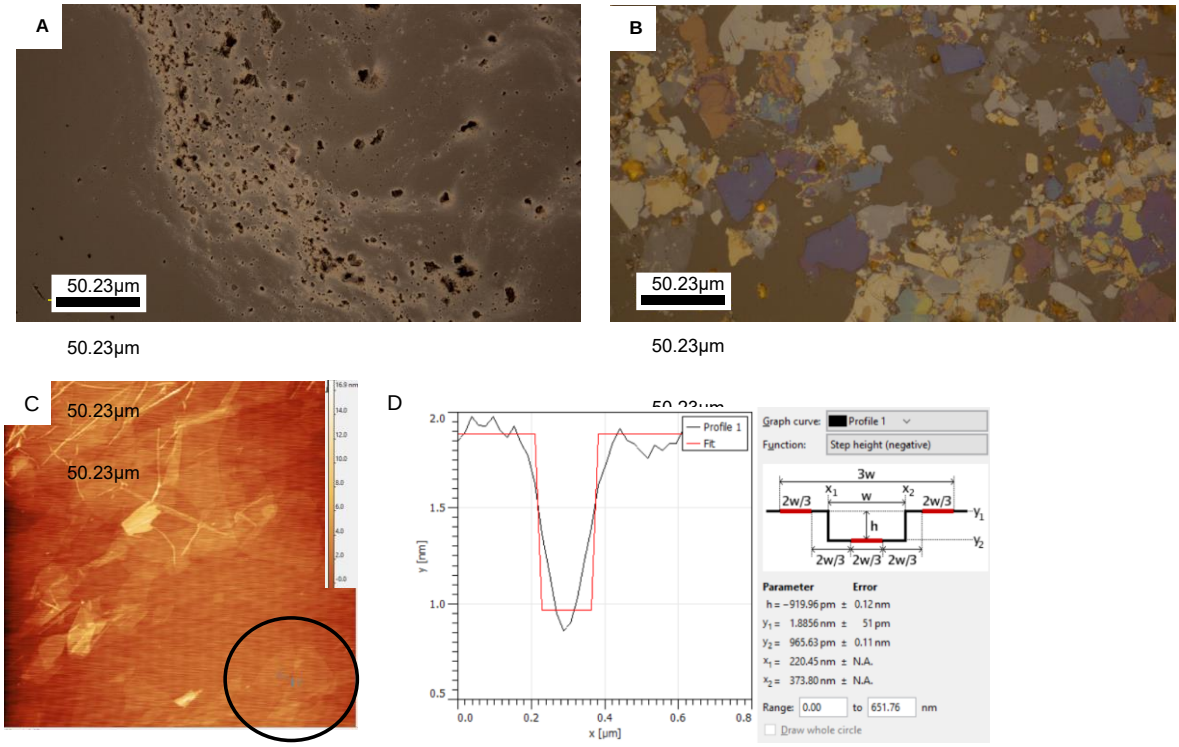


*Figure 6: Optical microscopy of graphene oxide thin film on glass slide. The old and the new GO synthesis methods are imaged (**A** and **B**). Atomic force microscopy height image (**C**) and profile height data (**D**).*

performed. GO was dispersed in nanopure water and allowed to settle overnight. Gravity pulled heavier multi-layer (undesirable) GO sheets to the bottom of the solution and the top portion was collected for application in aerogels. Single layer GO increased exposure of GO to polysiloxane emulsions resulting in a more even dispersion of polysiloxane on every sheet.

As previously mentioned, it is desirable to fully coat individual sheets for the purpose of the anode device. Many layer GO aggregates can be reoxidized in the same process for half the time duration to yield more oxidized and more single layer GO. Although this has been synthesized, a thorough study has not yet been conducted and will not be further discussed in this paper. Single layer GO have been observed under optical microscopy and atomic force microscopy (AFM), the results presented in Figure 6. Optical images show a high concentration of large, exfoliated GO sheets and AFM confirms the thickness of the single GO sheet to have the dimensions of a single layer GO sheet. Interesting properties have been observed by the single layer GO that was not present in the former GO material. Single layer GO forms a continuous transparent, reflective thin film, while MLGO layers are riddled with aggregates, Figure 6A.

Next, anode devices were fabricated with the decorated rGO, as described in the Methods section. Three cycle tests have demonstrated the capabilities of the anode devices. The results are presented in Figure 6. Initial cycle tests run for fully coated rGO sheets, Figure 6A, show

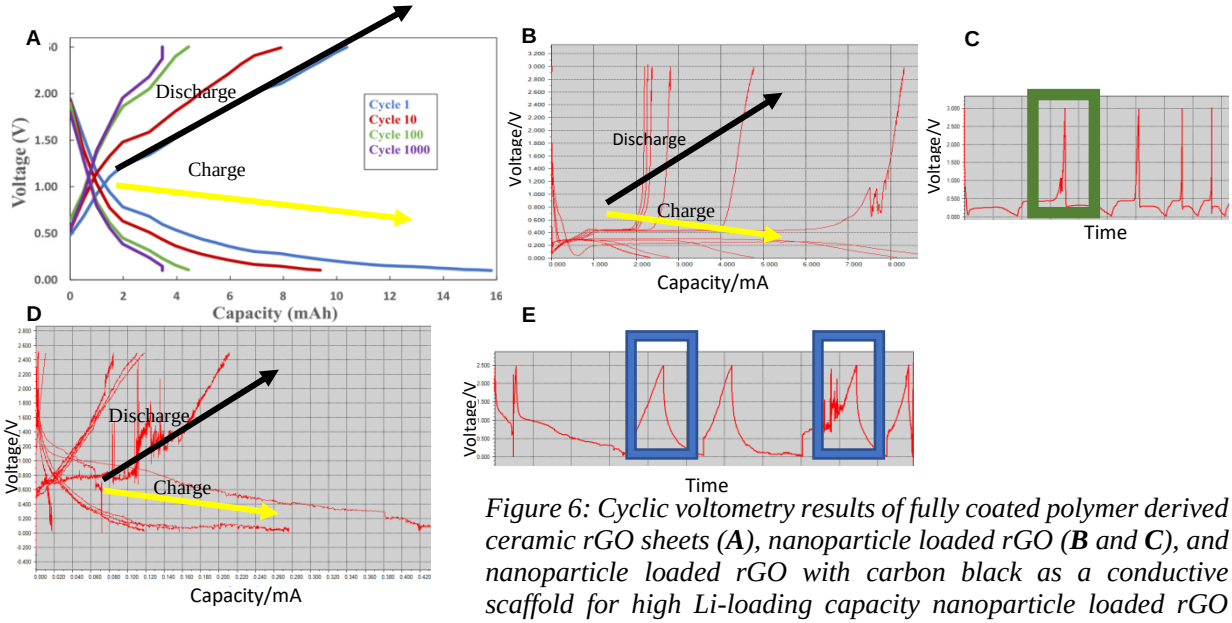


*Figure 6: Cyclic voltometry results of fully coated polymer derived ceramic rGO sheets (**A**), nanoparticle loaded rGO (**B** and **C**), and nanoparticle loaded rGO with carbon black as a conductive scaffold for high Li-loading capacity nanoparticle loaded rGO sheets (**D** and **E**).*

impressive capacitance, however, the device quickly failed to due intense internal resistance. Figure 7B-E show the same test, comparatively, with new nanoparticle loaded rGO. The anodes presented difficulty in stabilizing charge and discharge (7B and 7E). The anode device charge and discharge rates stabilized. The charge/discharge data suggest that the material deposited to form the electrode is not stable beyond 3-4 cycles, which is far from the 1000 cycles that would be required to consider the anode to be high performance. Further studies are in progress to understand the control of this system. Although nanoparticle loaded rGO sheets were confirmed, resistance between the sheets seems to pose a problem in the configuration considered in the scope of this work. It is important to note the changes observed from the green box in Figure 7C to the first blue box in Figure 7E where in 7C. In the green box, the anode device failed to stabilize and immedietly discharged during the delithiation phase. While this is important, the stability of the device is still limited as is observed in the second blue box in Figure 7C, where some changes in the anode device caused the failure of the battery.

The addition of carbon black in the loaded aerogel NMP slurry seemed to increase conductivity, suggesting that the lack of conductive pathways in heavily coated nanoparticle sheets may be one issue. Current efforts are aimed at utilizing the success of the carbon black material to replicate a similar process with a more compatible agent such as single layer rGO. By using single layer sheets, we hope to maintain the material individualized integrity while providing better conducting connective networks of rGO sheets. To test this, solutions of rGO and nanoparticle loaded rGO in NP are being synthesized with various ratios of the two solutions to determine the optimal conditions for the anode to operate.

Although only partially successful, the data is promising to form ideas moving forward. Other published works that used similar materials discussed paper anode device. This could be another avenue of development to test the performance of our material.

The properties of the material as a capacitor were also tested. Capacitance data on a parallel

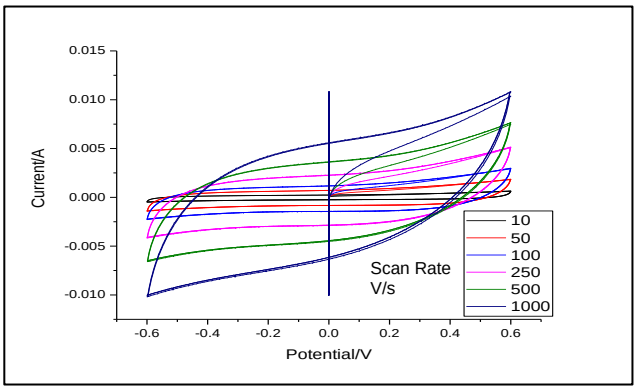


*Figure 8: Parallel plate capacitor tests revealing fast charge and discharge stable upwards of 500 V/s.*

plate capacitor is presented in Figure 8. The parallel plate capacitor exhibited promising charge and discharge rates. The device remained stable upwards of 500 V/s. Unfortunately, the material exhibited a very low capacitance of ~0.78 mF, calculated using Equation 1:

$$C = \frac{I\Delta t}{m\Delta V}$$

*Equation 1*

where C is the capacitance, I is the current, m is the mass of the active material, Δt is the scan rate over a period of time, and ΔV is the variance in potential in that time. We found that the capacitance is very low due to a large mass on the anode device of active material. This can be adjusted by making a thin film electrode for the capacitor or by using a paper electrode. Ultimately, if this device can be optimized as a capacitor, the material may become competitive for devices such as a supercapacitors.

# CONCLUSION

The results presented in the discussion provide some insight regarding the synthesis of new materials for energy devices. It is obvious that more research should be conducted to understand and control the system. Although anode devices have not yet been optimized, data collected using cyclic voltammetry and other similar materials [7,18] holds promise that this material could be successful as an anode device. Currently, the technology has been developed in such a manner that polymer derived ceramic nanoparticles have been coated on exfoliated single and few layer sheets. Future fabrication techniques will be employed to improve the performance of the electrode device as both a Lithium-ion battery anode and as a supercapacitor electrode. In order to improve the device as a battery electrode, it is hypothesized that increasing the connective network in the anode device, which was seen when carbon black was added to the material, will yield impressive results. The conductive material that will be used will be the same exfoliated rGO sheets in varying quantities to study the effect of limiting or increasing the conductive network and to find an optimal rGO and nanoparticle loaded rGO ratio for an anode device. The rGO sheets will act in a similar manner as the rGO in paper anodes which have been successfully produced by David, L. [7] and Kolathodi, M.S [18].

Currently, the material has been studied using aluminum as a current collector. It is more appropriate to utilize copper as a current collector for negative electrodes, therefore, future devices will be fabricated using copper current collectors. Comparatively, in anode tests shown in Figure 7B, 7C, 7D, and 7E when conductive carbon black was added, an improvement in the stability of the charge and discharge of the device was demonstrated. More work is required to stabilize the

capacitance of the device however over long cycles and to also stabilize the charge and discharge without experiencing shortages in the circuit.

Furthermore, electrode tests as a parallel plate capacitor have also demonstrated impressive qualities. This process will be tuned to optimize the poor capacitance and exploit the impressive charge and discharge rate of the supercapacitor. This will be executed by minimizing the coating on the carbon current collector. Although this material demonstrates impressive qualities as an electrode device, work to develop a functioning device will be ongoing and it is hopeful that this method will be an attractive replacement to existing methods [7,18] that utilize long chemical processes or ball-milling which provide minimal particle size control and dispersion and are time consuming.

# REFERENCES


1. An, S. J., Li, J., Sheng, Y., Daniel, C., Wood, D. L. (2016). Long-term lithium-ion battery performance improvement via ultraviolet light treatment of the graphite anode. *Journal of The Electrochemical Society*, *163* (14), A2866-A2875.
2. Aurbach, D. (2000). Review of selected electrode–solution interactions which determine the performance of Li and Li ion batteries. *Journal of Power Sources*, *89* (2), 206-218.
3. Birkl, C., Mcturk, E., Roberts, M., Bruce, G., Howey, D. (2015). A Parametric Open Circuit Voltage Model for Lithium Ion Batteries. *Journal of The Electrochemical Society*, 162. 2271-2280
4. Boukamp, B. A., Lesh, G. C., Huggins, R. A. (1981). All-solid lithium electrodes with mixed-conductor matrix. *Journal of The Electrochemical Society*, *128*(4), 725-729.
5. Burg, B., Schneider, J., Maurer, S., Niklas C. S., Poulikakos**,** D.. (2010). Dielectrophoretic integration of single- and few-layer graphenes. *Journal of Applied Physics*, 107, 034302.
6. Cairns, E.J., Albertus, P. (2010). Batteries for Electric and Hybrid-Electric Cars. *Annual Review of Chemical and Biomolecular Engineering*, 1, 299-320.
7. David, L., Bhandavat, R., Barrera, U., Singh, G. (2016). Silicon oxycarbide glass-graphene composite paper electrode for long-cycle lithium-ion batteries. *Nature communications*, *7*.

8. Delpuech, N., Dupr´e, N., Mazouzi, D., Gaubicher, J., Moreau P., Bridel, J. S., Guyomard, D., Lestriez, B. (2013). Critical role of silicon nanoparticles surface on lithium cell electrochemical performance. *J. Phys. Chem. C*. 33, 72–75.

9. Deville, S., Saiz, E., Tomsia, A.P. (2006). Freeze casting of hydroxyapatite scaffolds for bone tissue engineering. *Biomaterials* 27 5480-4489.

10. Fukasawa, T., Deng, Z.Y., Ando, M., Ohji, T., Goto, Y. (2001) Pore structure of porous ceramics synthesized from water-based slurry by freeze-dry process. *J Materials Science*, 36, (10) 2523–2527.

11. Hu, Y. S. (2016). Batteries: getting solid. *Nature Energy*, *1*, 16042.

12. Jiang, F., Peng, P. (2016). Elucidating the Performance Limitations of Lithium-ion Batteries due to Species and Charge Transport through Five Characteristic Parameters. *Scientific Reports*, *6*, 32639.

13. Kalnaus, S., Rhodes, K., Daniel, C. (2011). A study of lithium ion intercalation induced fracture of silicon particles used as an anode material in Li-ion battery. *J. Power Sources*, 196, 8116–8124

14. Kang, H.W., Tabata, Y., Ikada, Y. (1999). Fabrication of porous gelatin scaffolds for tissue engineering. *Biomaterials*, 20 (14), 1339–44.

15. Kang, J.H., Kim, T., Choi J., Park, J., Kim, Y.S., Chang, M.S., Jung, H., Park, K.T., Yang, S.J. C.R. (2016) Hidden Second Oxidation Step of Hummers Method Park *Chemistry of Materials 28* (3), 756-764.

16. Kannan, A. G., Kim, S. H., Yang, H. S., Kim, D. W. (2016). Silicon nanoparticles

grown on a reduced graphene oxide surface as high-performance anode materials for lithium-ion batteries. *RSC Advances*, *6*(30), 25159-25166.

17. Key, B., Bhattacharyya, R., Morcrette, M., Seznec, V., Tarascon, J. M., Grey, C. P. (2009). Real-time NMR investigations of structural changes in silicon electrodes for lithium-ion batteries. *Journal of the American Chemical Society*, *131*(26), 9239-9249.

18. Kolathodi, M.S., David, L., Abass, M.A., Singh, G. (2016). Polysiloxane-functionalized graphene oxide paper: pyrolysis and performance as Li-ion battery and supercapacitor electrode. *RSC Advances 78* (4) 54-63

19. Kumar, B.M., Kim, Y.W. (2010). Processing of polysiloxane-derived porous ceramics: a review. *Science and Technology of Advanced Materials* (4) 11, 044303.

20. Larcher, D., Beattie, S., Morcrette, M., Edström, K., Jumas, J.-C., Tarascon, J.-M. (2007). Recent findings and prospects in the field of pure metals as negative electrodes for Li-ion batteries. *Journal of Materials Chemistry*, *17*(36), 3759.

21. Liu, X. H., Zhong, L., Huang, S., Mao, S. X., Zhu, T., & Huang, J. Y. (2012). Size-dependent fracture of silicon nanoparticles during lithiation. *Acs Nano*, *6*(2), 1522-1531.

22. Lu, L., Han, X., Li, J., Hua, J., Ouyang, M. (2013). A review on the key issues for lithium-ion battery management in electric vehicles. *Journal of power sources*, *226*, 272-288.

23. Manthiram, A., Yu, X., Wang, S. (2017). Lithium battery chemistries enabled by solid-state electrolytes. *Nature Reviews Materials*, *2*, 16103.

24. Marques, E.F. (2000). Sizze and Stability of Catanionic Vesicles: Effects of Formation Path, Sonication, and Aging. *Langmuir* 16 (11) 4798-4807.

25. McDowell, M. T., Lee, S. W., Nix, W. D., Cui, Y. (2013). 25th anniversary article: Understanding the lithiation of silicon and other alloying anodes for lithium-ion batteries. *Advanced Materials*, *25*(36), 4966–4985.

26. Narisawa, M. (2010). Silicone Resin Applications for Ceramic Precursors and Composites. *Materials (Basel,)* 3(6) 3518-3536

27. Nie, M., Abraham, D. P., Chen, Y., Bose, A., Lucht, B.L. (2013). Litihum Ion Battery Graphite Solid Electrolyte Interphase Revealed by Microscopy and Spectroscopy. *J. Phys. Chem*, 117, 1257-1267.

28. Oumellal Y., Delpuech, N., Mazouzi, D., Dupr´e, N. J. Gaubicher, N., Moreau, P., Soudan, P., Lestriez, B., Guyomard, D. (2011). The failure mechanism of nano-sized Si-based negative electrodes for lithium ion batteries. *J. Mater. Chem.*, 21, 6201–6208.

29. Pradeep, V.S., Zajac, M.G., Riedel, R., Soraru, G.D. (2014). New Insights in to the Lithium Storage Mechanism in Polymer Derived SiOC Anode Materials. *Electrochimica Acta 119* (4), 78-85.

30. Rahman, M. A., Song, G., Bhatt, A. I., Wong, Y. C., Wen, C. (2016). Nanostructured silicon anodes for high-performance lithium-ion batteries. *Advanced Functional Materials*, *26*(5), 647–678.

31. Rodrigues, M. T. F., Babu, G., Gullapalli, H., Kalaga, K., Sayed, F. N., Kato, K.,

Ajayan, P. M. (2017). A materials perspective on Li-ion batteries at extreme temperatures. *Nature Energy*, *2*, 2017108.

32. Tahir, M. S., Weinberger, M., Balasubramanian, P., Diemant, T., Behm, R. J., Lindén, M., Wohlfahrt-Mehrens, M. (2017). Silicon carboxylate derived silicon oxycarbides as anodes for lithium ion batteries. *J. Mater. Chem. A*, *5*(21), 10190–10199.

33. Shi, L., Pang, C., Chen, S., Wang, M., Wang, K., Tan, Z., Gao, P., Ren, J., Huang, Y., Peng, H., Liu, Z. (2017). Vertical Graphene Growth on SiO Microparticles for Stable Lithium Ion Battery Anodes. *Nano Letters*, *17*(6), 3681–3687.

34. Yu, Z., McInnis, M., Calderon J., Thomas, J. Functionalized graphene aerogel composites for high-performance asymmetric supercapacitors. *Nano Energy*, 11, 611-620.

35. Zhang, W. J. (2011). A review of the electrochemical performance of alloy anodes for lithium-ion batteries. *Journal of Power Sources*, *196*(1), 13-24.